Measuring Charge Carrier Diffusion in Coupled Colloidal Quantum Dot Solids

David Zhitomirsky,[†] Oleksandr Voznyy,[†] Sjoerd Hoogland, and Edward H. Sargent*

Department of Electrical and Computer Engineering, University of Toronto, 10 King's College Road, Toronto, Ontario, M5S 3G4, Canada. [†]D.Z. and O.V. contributed equally to this work.

ABSTRACT Colloidal quantum dots (CQDs) are attractive materials for inexpensive, room-temperature-, and solution-processed optoelectronic devices. A high carrier diffusion length is desirable for many CQD device applications. In this work we develop two new experimental methods to investigate charge carrier diffusion in coupled CQD solids under charge-neutral, *i.e.*, undepleted, conditions. The methods take advantage of the quantum-size-effect tunability of our materials, utilizing a smaller-bandgap population of quantum dots as a reporter system. We develop analytical models of diffusion in 1D and 3D structures that allow direct extraction of diffusion length from convenient parametric plots and purely optical measurements. We measure several CQD solids fabricated using a number of distinct methods and having significantly different doping and surface ligand treatments. We find that CQD materials recently reported to achieve a certified power conversion efficiency of 7% with hybrid organic–inorganic passivation have a diffusion length of 80 ± 10 nm. The model further allows us to extract the lifetime, trap density, mobility, and diffusion coefficient independently in each material system. This work will facilitate further progress in extending the diffusion length, ultimately leading to high-quality CQD solid semiconducting materials and improved CQD optoelectronic devices, including CQD solar cells.

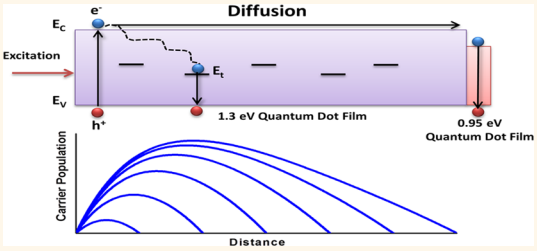

KEYWORDS: colloidal quantum dots · diffusion length · mobility · lifetime · transport

Colloidal quantum dots (CQDs) are nanocrystal particles dispersed in solution, synthesized and rendered colloidally stable typically with the aid of long aliphatic ligands. CQDs' bandgap can be tuned simply by changing nanoparticle size at the time of synthesis, a distinct advantage over bulk semiconductors. In an effort to exploit CQD films' solution-processability and tunable electronic properties, researchers have deployed these materials in light-emitting diodes,[1−3] photodetectors,[4−6] and photovoltaic devices.[7−10] Recently, CQDs selected to have the optimal single-junction solar cell bandgap of ∼1.3 eV were used to build a solar cell having a certified 7% power conversion efficiency.[8]

Fabricating CQD solids for optoelectronic device applications relies on increasing the electronic coupling among neighboring nanocrystals. To accomplish this, the long native ligands are displaced by more strongly binding short ligands, bringing the CQDs into more intimate electronic coupling *via* a reduction in the interdot spacing. It has been shown that charge carrier mobility in these materials is highly dependent on the coupling,[2,11] while the recombination dynamics and lifetime depend strongly on the type and degree of passivation.[8,12] Maximizing both the transport properties of charge carriers, and also their recombination lifetimes, is essential to achieve further advances in device applications.

The distance over which a photoinduced excitation can diffuse before it recombines, the diffusion length, is a crucial parameter in an electronic material. It is influenced by both transport and recombination and may proceed by energy transfer or transport of free electrical charges. Specifically, in the case of minority carrier diffusion in the low-level injection approximation, the diffusion length (L_D) is given by the square root of the product of the diffusion coefficient and the charge carrier lifetime. It is of wide importance in crystalline, polycrystalline, and disordered semiconductors alike CQDs.[13−15]

Since all high-performing solar cells include a quasi-neutral region, a volume of light-absorbing material in which the electric field plays a minimal role, this diffusion

* Address correspondence to ted.sargent@utoronto.ca.

Received for review March 2, 2013 and accepted May 23, 2013.

Published online May 23, 2013
10.1021/nn402197a

length becomes an important parameter in device performance.[16]

Multiple recent reports on charge transport have relied on field effect transistor (FET) studies. In FET mobility measurements, the Fermi level is moved through the bandgap, often to an extent unprobed in solar cells under 1 sun illumination levels.[17−19] For this reason, it is not immediately clear the mobility values reported in FET studies bear directly on diffusion lengths experienced in operating solar cells. Studies that use the FET mobility, combined with the Einstein relation $D = kT\mu/q$ and independent measures of charge carrier lifetimes,[12,20−22] have led to a wide dispersion in reported results for ostensibly similar materials. They have also typically produced L_D values that were vastly longer than what photovoltaic performance-oriented device studies would suggest.

More direct measures of diffusion lengths are thus desired. Studies based on short circuit current resulting from optical excitation were employed for this purpose.[23−25] Such techniques require building a p-n junction test structure with specific electrical contacts and a compatible materials interface. The electron beam induced current technique is commonly employed for bulk semiconductors which employs an electron rather than photon source but has limitations at nanometer length scales.[26] In other material systems, impedance spectroscopy has been employed to determine the diffusion lengths.[27] Here, an exact electrical model is needed to interpret the experimental results. Techniques based on heterojunction photoconductance measurements in polymer/TiO_2 structures have successfully yielded diffusion lengths but require measuring time-resolved microwave conductivity.[28,29] In this work, we report two new, direct methods of measuring L_D experimentally in CQD materials. These new methods were designed purely on the light-absorbing film, removing all contact and interface effects. They are the first to take advantage of the CQD bandgap tunability and observation of the direct photoluminescence (PL) signal from the CQDs to measure directly the action of diffusing carriers.

RESULTS AND DISCUSSION

Probing Diffusion Using the 1D Method. We sought to develop a method of directly measuring the diffusion length. As doping densities in CQD materials are reported on the order of 10^{16} cm^{-3},[30] transport in these materials under 1 sun illumination occurs in the low-level injection approximation and is dominated by minority carrier diffusion. Under high injection scenarios that could also be studied with higher illumination intensity or lower-doped films, ambipolar drift-diffusion ensures that the less-diffusive carrier dominates the observed diffusion length.[31]

Our approach involved exciting photocarriers in a known spatial distribution (determined by the material's (known, measured) optical absorption coefficient at the chosen excitation wavelength) within the CQD film (Figure 1a). We would do so under steady-state conditions, with intensities similar to solar intensities. This would approximate closely the conditions at work within operating solar cells. The excess photogenerated charge carriers would then diffuse in the film, and we would seek to detect the efficiency with which they arrived at an end point a known distance from the location of generation. Specifically, we situated a luminescent reporter, which we refer to as the acceptor (Figure 1a, right-hand-side), immediately on top of the donor layer in which transport was to be studied. In creating the acceptor from a CQD film, we leveraged quantum size-effect tuning[32] to produce a medium having a distinct PL spectral signature relative to the donor,[33,34] in contrast to similar one-dimensional methods in organic semiconducting materials where quenching of the PL is used to determine the diffusion length.[35,36] We refer to this configuration throughout the present work as the 1D method.

At steady state ($dn(x)/dt = 0$, where n is the carrier concentration), we can solve the following equation in 1D to represent the carrier profile:

$$Dn(x)'' - \frac{n(x)}{\tau} = -g(x) \qquad (1)$$

where D is the diffusion coefficient, τ is the carrier lifetime, and g is the generation rate. The solution of this equation for a monochromatic excitation has the form:

$$n(x) = Ae^{-x/L_D} + Be^{x/L_D} + Ce^{-\alpha x} \qquad (2)$$

where α is the absorption coefficient, L_D is the diffusion length, and A, B, and C are constants. Importantly, these constants are a function of sample thickness d, and hence the carrier profile will depend on the choice of sample thickness.

To obtain solutions specific to our 1D configuration, we now impose quenching boundary conditions, where $n(x) = 0$ on both sides, leading to

$$C = -\frac{\alpha}{D\alpha^2 - \frac{1}{\tau}}, \quad A = C\frac{-e^{-\alpha d} + e^{d/L_D}}{e^{-d/L_D} - e^{d/L_D}},$$

$$B = C\frac{-e^{-\alpha d} + e^{-d/L_D}}{e^{d/L_D} - e^{-d/L_D}}$$

The form of the solutions is illustrated in Figure 1b, top panel, for a range of thicknesses. The rate of rise of the carrier population is related to $1/\alpha$, the absorption length, and the rate of fall to the right directly related to L_D.

The measured signal in this experiment is the PL intensity in the acceptor, which in turn is related to the flux across the donor−acceptor boundary. Figure 1b), bottom panel, shows the model-predicted

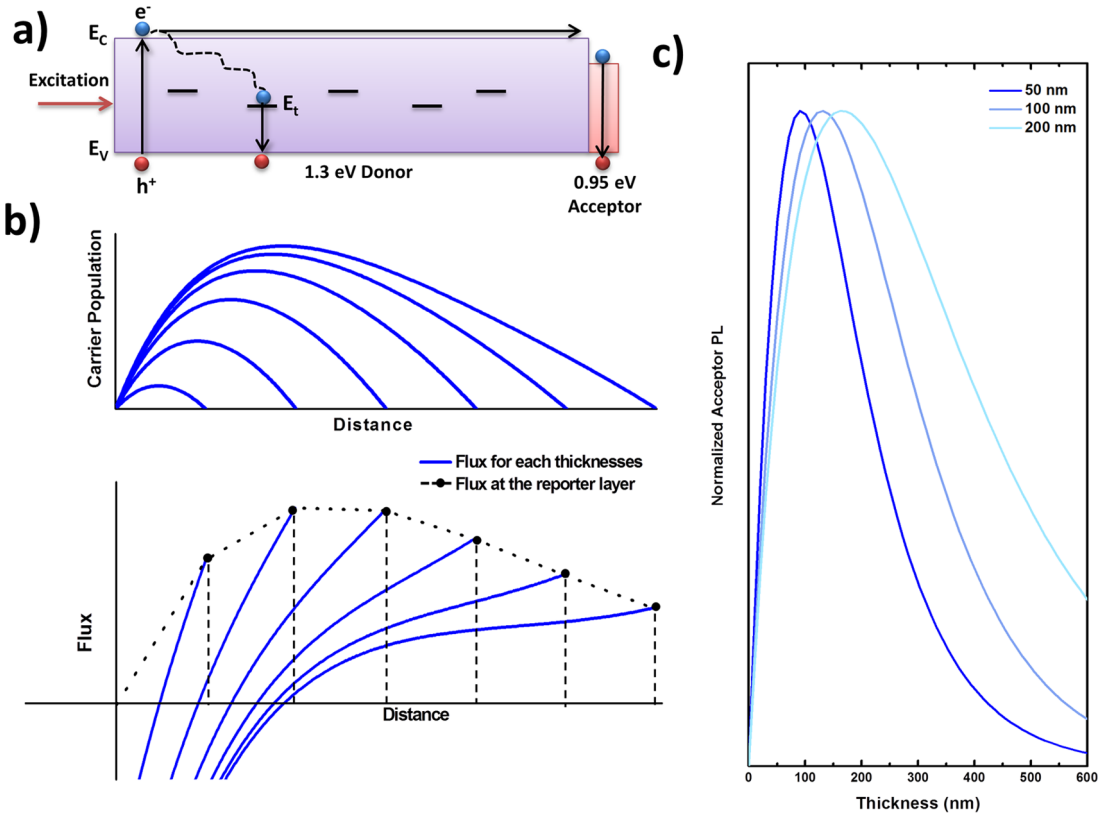

Figure 1. The 1D diffusion method. (a) A donor layer is illuminated on one end, generating a charge carrier profile with the material. Carriers diffuse across the donor and eventually recombine in the acceptor unless they recombine *via* the band-edge or trap-level. (b) Carrier populations and flux (defined in the positive direction) obtained for several simulated film thicknesses employing the 1D model. (c) Several flux envelopes plotted for different diffusion lengths, indicating the envelope broadens as diffusion length is increased.

carrier flux (defined in the positive direction) as a function of position for several thicknesses, given a fixed L_D. The terminal point (black circles) ending each curve is the flux, hence proportionately the PL signal, expected at the beginning of the small-bandgap CQD quenching layer. These points form an envelope that represents the flux from a sample with a fixed L_D as a function of sample thickness, which can then be used to fit experimental data and extract L_D. The equation for the flux at the far boundary of a film of fixed thickness d is

$$\mathrm{PL}_{\mathrm{Flux}} = -Dn'(x = d) = \frac{1}{L_D}\left(Ae^{-d/L_D} - Be^{d/L_D}\right) + \alpha C e^{-\alpha d} \quad (3)$$

Figure 1c) shows several such envelopes modeled with different L_D according to eq 3, showing that as L_D improves, the flux envelope broadens and maintains a greater magnitude at increased thicknesses.

We instantiate the above framework in an experiment where 1.3 eV bandgap (950 nm) CQDs comprise the donor (diffusive transport) layer, while a single, thin layer of smaller-bandgap (0.95 eV, 1300 nm) CQDs are used as the acceptor (quencher and reporter). Figure 2a shows the acceptor spectra obtained for varying the thickness of the donor (PL peak is at 1400 nm due to Stokes shift[37]). As the thickness of the donor is increased, the acceptor PL decreases, consistent with fewer carriers reaching the boundary. The acceptor PL is measured as a function of donor layer thickness. We investigated CQD films cross-linked using the bifunctional organic molecule mercaptopropionic acid (MPA, organic-cross-linked);[30] for recently reported all-inorganic, halide-treated PbS CQDs (all-inorganic);[38] and for an organic−inorganic passivation approach (hybrid).[8] The fitting procedure is carried out according to eq 3 to extract L_D for these materials (Figure 2b), where sample spectra are shown for the organic-cross-linked (Figure 2c), hybrid (Figure 2d), and inorganic (Figure 2e) films, to highlight the broadening of the flux envelopes observed for materials with a substantially different diffusion length.

We then used our method to investigate the advantages of a recent advance in CQD film-forming materials processing. It was recently reported that photovoltaic device performance was dramatically improved when the organic cross-linking was augmented using an initial halide salt passivation step during CQD synthesis.[8] Here we find that a comparably large difference in L_D separates the organic-cross-linked films (L_D = 30 nm ± 10 nm) from hybrid

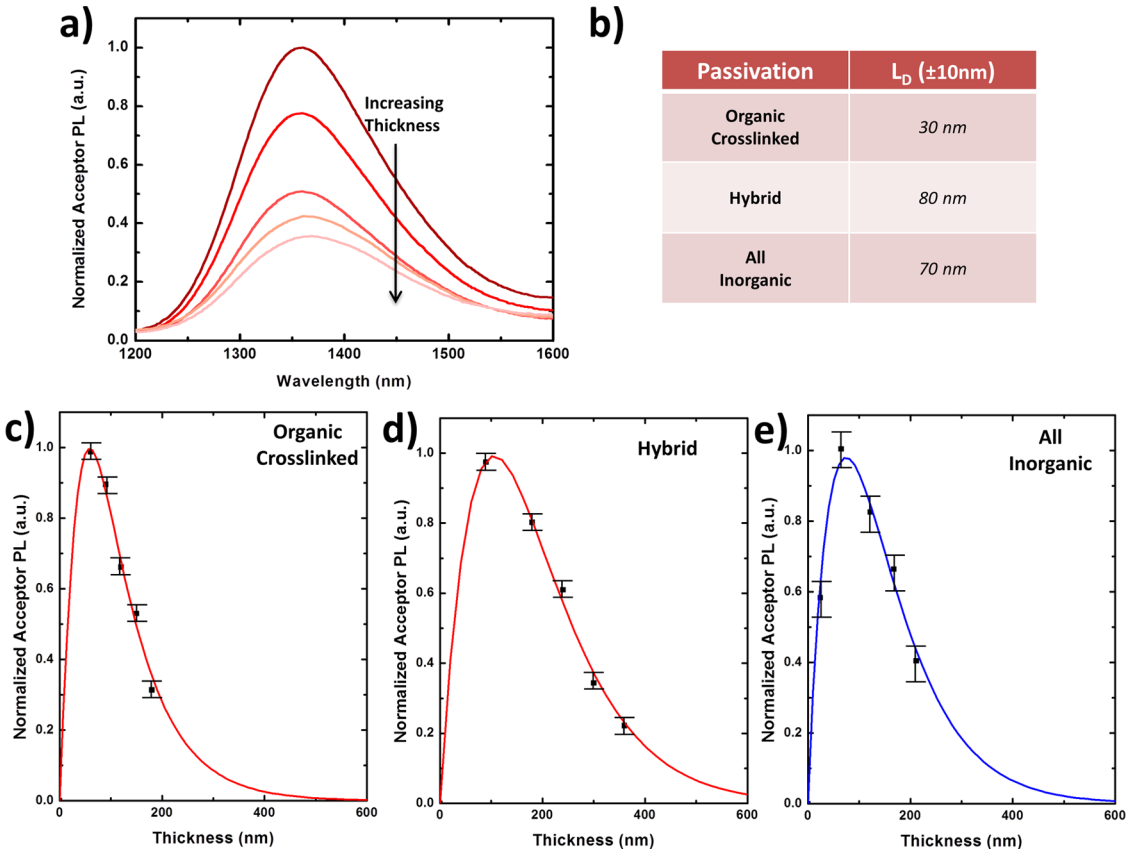

Figure 2. Experimental results from the 1D method. (a) PL from the acceptor layer for various thicknesses of donor layer. (b) Summary of extracted diffusion lengths for various materials employed in the 1D scenario. Acceptor PL/flux measurements done for (c) organic-cross-linked (d) hybrid films and (e) all-inorganic films, with the fit according to eq 3.

(organic-cross-linked, halide-treated) films (L_D = 80 nm ± 10 nm) CQDs. The large diffusion length in the all-inorganic CQD films helps account for excellent performance of another recently reported solar cell architecture employing a p-n junction comprised entirely of PbS CQDs, where each side of the junction can be quantum-size-effect-tuned[7] (L_D = 70 nm ± 10 nm). The standard deviation of ±10 nm was obtained by evaluating the results of six separate trials employing different dot batches and nominally identical synthesis, processing, and automated data analysis.

The benefit of the 1D method is its directness in providing an explicit measure of diffusion length and its improvement in superior CQD materials. We note, however, that it does not allow us to attribute the improvement to better transport, delayed recombination, or some combination thereof.

Probing Diffusion Using the 3D Method. We sought to develop a method of analysis, ideally one as convenient as the 1D method, that would allow L_D, and also its constituent diffusivity (D) and lifetime (τ) factors, to be separately determined.

Our concept for so doing is depicted in Figure 3a) and is referred to as the 3D method. Our notion was that traps, into which diffusing charge carriers are readily captured and from which they are challenged by a thermionic emission barrier to escape, already play a potentially significant role in charge carrier diffusion. We postulated that the controlled addition of a carefully quantitated population of additional traps, in the form of small-bandgap CQDs, could offer an additional and systematically varied experimental degree of freedom that would allow us to extract independent, transport related parameters with a minimum of assumptions.

Such a method could be expected to provide a measure of diffusion length, since in poor-transport materials, the average photocarrier would recombine before it reached the reporter small-bandgap (acceptor) dot (Figure 3b); while in materials having a transport length exceeding the average interacceptor dot distance, the average photocarrier would reach the acceptor and recombine therein, emitting its characteristic PL spectral signature (Figure 3c).

An initial experiment (Figure 3d) confirmed this picture. Two films were made, each "doped" using 1% by mass with small-bandgap 0.95 eV acceptor dots; the preponderance of the film (99%) consisted of the same transport-phase (donor-phase) 1.3 eV dots as employed up to this point in the 1D studies. When poorly electronically coupled films were created by preserving the long insulating oleic-acid ligands

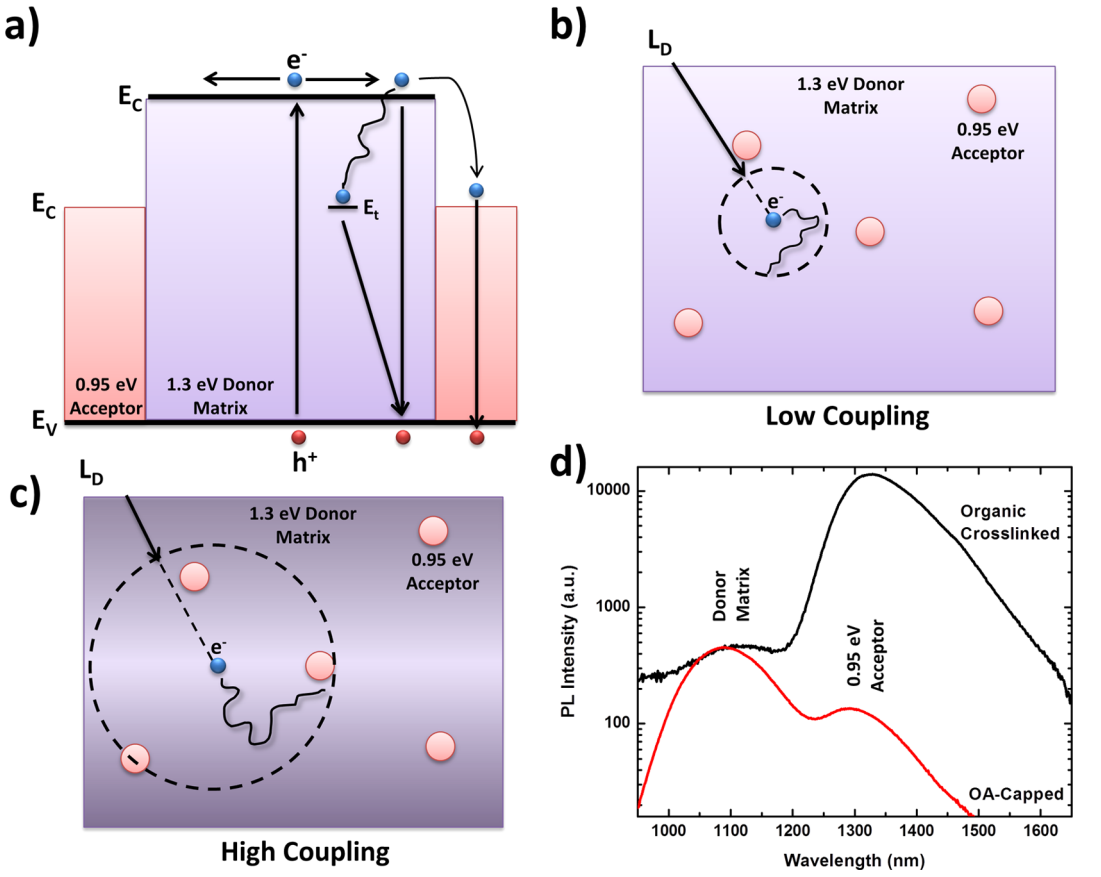

Figure 3. The 3D diffusion method. (a) Energy band diagram of donor and acceptor material and transport and recombination pathways a charge carrier may undertake when generated in the donor host material. (b) Macroscopic depiction of the low coupling scenario where the average delocalization of the carrier is small compared to the distance to an acceptor. (c) High coupling scenario where the delocalization distance is large and hence carrier can recombine through acceptor sites. (d) PL of Organic-cross-linked and OA-capped films normalized at exciton showing the impact of adding 1% smaller bandgap inclusions.

(OA-capped) with which the dots were synthesized, luminescence was primarily from the donor matrix (Figure 3a, red curve). In contrast, when the dots were coupled using the MPA-based ligand exchange that has led to the highest photovoltaic device performance, the rare, lower-energy "quantum traps"[39] acting as acceptors dominated luminescence (Figure 3a, black curve, ~1400 nm emission). Similar mixes of materials with different bandgaps have been studied in nanocrystals[40] and organics;[41] however, extraction of diffusion and other transport related properties was not carried out.

Encouraged by this preliminary qualitative result, we attempted to build a simple 3D quantitative model that might offer possibilities for the extraction of additional parameters. We introduced three energy levels: the CQD matrix; the intentionally introduced smaller-bandgap acceptor CQDs; and the traps native to the donor matrix, often attributed to surface defects or impurities.[8,39,42,43] The carrier population change in time is written as

$$\frac{dn}{dt} = G - \frac{n}{\tau_{bandedge}} - \frac{n}{\tau_{acceptor}} - \frac{n}{\tau_{traps}} \quad (4)$$

Where at steady state this is equal to zero, *i.e.*, generation will equal recombination. The first recombination term represents bandedge PL. The second represents a rate capture from bandedge donor states into acceptors and does not account for escape. The third similarly represents capture into traps native to the donor matrix.

We expressed the capture rate into traps as $V_{th}\sigma N_t$, where N_t can represent the trap or acceptor concentrations, where V_{th} is the thermal velocity, and σ is the capture cross section. In a hopping regime, we can express $V_{th} = d/\tau_{hop}$, where d is the interdot distance, mobility as $\mu = qd^2/6\tau_{hop}kT$,[15] where τ_{hop} is the dot-to-dot hopping time; from these equations we find $V_{th} = 6\,D/d$. We define the acceptor-to-donor PL ratio and solve to obtain

$$PL_{RATIO} = \frac{PL_{ACCEPTOR}}{PL_{BANDEDGE}} = \frac{\frac{n}{\tau_{acceptor}}}{\frac{n}{\tau_{bandedge}}} = \frac{\tau_{bandedge}}{\tau_{acceptor}}$$

$$= [\tau_{bandedge} \times 6kT\mu(qd)^{-1}\sigma]N_A \quad (5)$$

This ratio is linear with the acceptor concentration (N_A), suggesting an experiment in which N_A is varied

and the quantity $\tau_{bandge} \times 6kT\mu(qd)^{-1}\sigma$ extracted as the slope, S, of the PL_{RATIO} *versus* N_A plot. The diffusion coefficient can thence be obtained:

$$D = \frac{Sd}{\tau_{bandedge} 6\sigma} \quad (6)$$

as long as the capture cross-section is estimated, for which purpose we approximated the cross-section by the CQD side-view area, $\sigma = {}^1/_4\pi d^2$.

The effective lifetime of the pure-phase donor material (*i.e.*, without the artificially introduced acceptor inclusions) is given by $\tau_{effective}{}^{-1} = \tau_{bandedge}{}^{-1} + \tau_{traps}{}^{-1}$. Since the radiative lifetime in PbS CQDs is 1−10 μs, but reported films exhibit sub-μs lifetimes,[12] the effective lifetime is trap-dominated, hence from equations 5, 6

$$\tau_{effective} \sim \tau_{traps} = \frac{\tau_{bandedge}}{S \times N_t} \quad (7)$$

Thus the lifetime may be extracted without assuming an estimated cross-section. Finally, to extract the trap density inherent to the donor medium, we note that the total recombination rate is equal the generation rate, the latter a conserved quantity among the different experiments in view of the fixed absorbance and fixed excitation conditions:

$$\begin{aligned} PL_{TOTAL} &= PL_{bandedge} + PL_{acceptor} + PL_{trap} \\ &= PL_{bandedge} + PL_{acceptor}\left(1 + \frac{N_{trap}}{N_{acceptor}}\right) \end{aligned} \quad (8)$$

Solving eq 8 as a system of equations for two experimental data points yields

$$N_t = \frac{PL_{bandedge1} - PL_{bandedge2} + PL_{acceptor1} - PL_{acceptor2}}{\frac{PL_{acceptor2}}{N_{A2}} - \frac{PL_{acceptor1}}{N_{A1}}} \quad (9)$$

where numerical designations correspond to samples with differently chosen acceptor inclusion concentrations N_A; several such calculations based on different pairs of points may be averaged to yield a good approximation of N_t. We obtain the diffusion length using the above-extracted parameters,

$$L_D = \sqrt{D\tau_{effective}} \quad (10)$$

and note that explicitly obtaining this quantity will allow comparison with the results of the simpler 1D model.

We now turn to a series of experimental studies aimed at deploying the 3D model developed above. We build CQD films using OA-capped CQDs (Figure 4a) and organic-cross-linked CQDs (Figure 4b) to provide examples of weakly and strongly coupled materials; similar spectra for the highly coupled hybrid material are shown in the Supporting Information (S2). The PL intensities of the pure acceptor and donor phases are of the same order of magnitude but differ in detail due to the combination of differences in transport properties as well as in bandedge and nonradiative recombination.[44] To challenge the applicability of the 3D model to the greatest extent feasible, we used 3 orders of magnitude of acceptor concentration, including a very low concentration designed to minimally impact the transport parameters of the medium (Supporting Information (S2)). We note that for intermediate concentrations of acceptor inclusions in highly coupled films (Figure 4b), the PL from inclusions is significantly higher than the pure donor or acceptor films. When the acceptor inclusions are added, charge carriers are rapidly conveyed to them and can recombine in them. Notably, when the concentration of the acceptor phase is in the range of 10%, the total luminescence from the sample is maximized. We explain this in terms of the rapid and efficient transport from the donor to isolated islands of the acceptor phase or nonradiative traps. In the pure phase, carriers will diffuse and preferentially recombine in deep nonradiative centers as opposed to the bandedge. When the acceptors are introduced, they irreversibly trap carriers and force them to recombine radiatively, reducing the migration of carriers into nonradiative centers. At lower (*e.g.*, 1% acceptor) concentrations, the effect is less remarkable since the amount of acceptors is lowered. In the pure acceptor phase, photocarriers are able to diffuse and find nonradiative centers again, thus diminishing the bandedge PL, similarly to pure donor phase. This suggests that low PL quantum yield of coupled films is not due to inherently poor passivation during ligand exchange but rather due to improved transport which allows carriers to find and recombine in rare but highly recombinative trap states in the film, as has been reported in related works.[2,12,22,44]

We used eq 6 to extract mobility (Figure 4c). Obtaining an absolute value required an estimate of the CQD density in the donor, which we determined to be 1.5×10^{19} cm^{-3} based on the cube of the inverse radius of the CQDs as well as published literature.[45] Figure 4d shows the trap density calculated according to eq 9, where the error bars are based on multiple repeated nominally identical experiments. Additional transport and lifetime parameters are also provided (Supporting Information (S3)). Finally, L_D reported in Figure 4e) is obtained using the aforementioned extracted parameters applied in eq 10.

OA-capped CQDs have, as expected, a very poor mobility below 10^{-4} cm^2/(V s) and, more interestingly, a very low trap density. To our knowledge, this method, based on the systematic inclusion of experimentally varied acceptors, is the first to allow the extraction of the trap density in such a weakly coupled material, in which established methods (such as V_{OC} transient[46,47]) are not available. It is usually assumed in the literature that for weakly coupled CQD films, Förster resonance

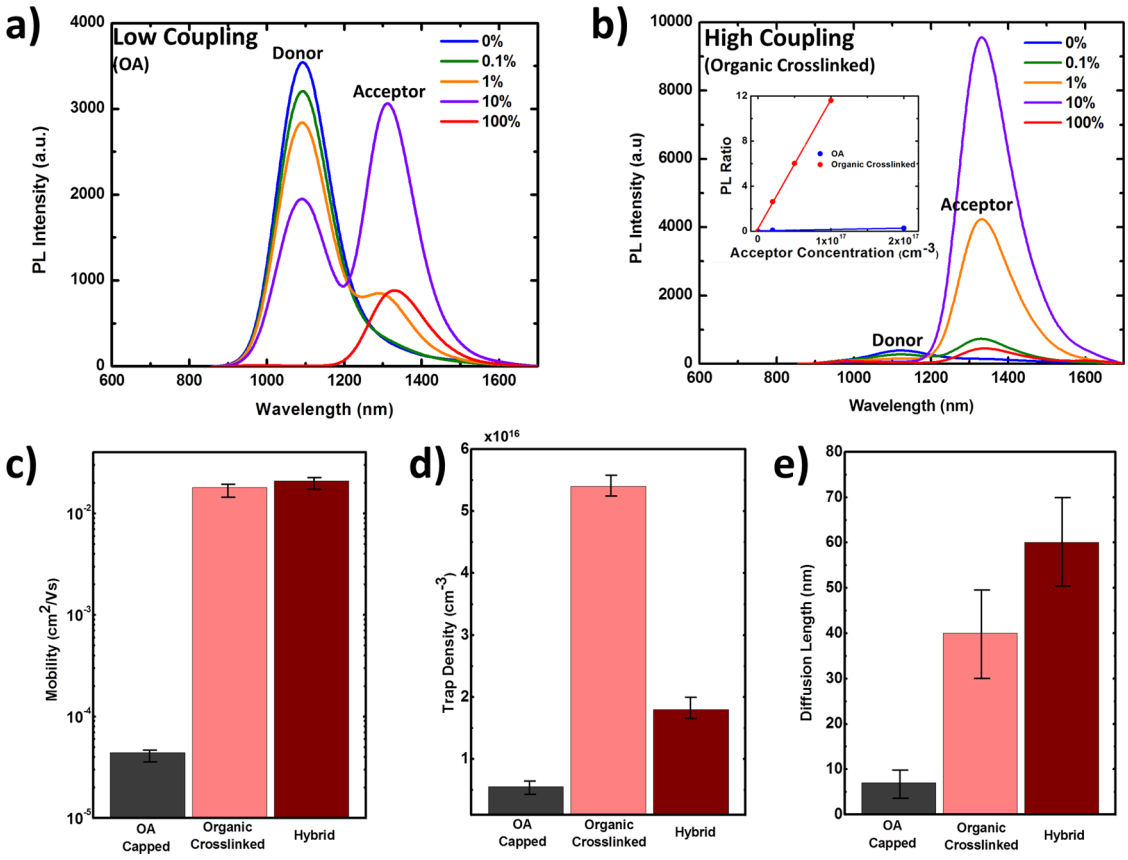

Figure 4. Experimental results from the 3D method. PL spectra for (a) OA-capped and (b) organic-cross-linked CQD films with a given percentage of small bandgap inclusions, showing the charge transfer under the various coupling regimes. The inset shows sample PL ratios for low (OA) and highly coupled (organic cross-linked) materials as a function of acceptor concentration. Extracted (c) mobility, (d) trap density, and (e) diffusion length for several types of PbS CQD solid films.

energy transfer (FRET) is the main transport mechanism.[12,40] Therefore, in the OA-capped case, we likely measure the exciton diffusion length rather than minority carrier diffusion length. The transport measurement methods employed herein apply equally well to minority carrier diffusion as to exciton diffusion, as explained in the Supporting Information (S4). Additionally, since energy transfer is a downhill process it can only proceed a small number of times before no nearest-neighbor lower-energy acceptors are available. We thus interpret diffusion lengths exceeding 10 nm as dominated by minority carrier diffusion.

The diffusion length observed for hybrid PbS CQD materials (60 nm ± 10 nm) exceeds that in the organic-cross-linked (40 nm ± 10 nm) materials. It also agrees, within experimental error, with the independently obtained diffusion length from the 1D method.

The 3D method has the notable advantage of allowing independent information about transport and recombination. The mobility in the organic-cross-linked *versus* the hybrid material is the same to within experimental error. In contrast, the trap density is 3-fold higher in the organic-only material ($1.8 \times 10^{16} \pm 2 \times 10^{15}$ cm^{-3} *versus* $5.4 \times 10^{16} \pm 2 \times 10^{15}$ cm^{-3}), though such fitting is sensitive to the choice of σ but still allows for a meaningful relative comparison. Thus, the 3D method allowed us to determine that the advantage of the hybrid scheme is primarily in passivation, rather than in mobility. We note that this finding, and also the quantitative estimates of trap densities, agree well with the V_{OC} transient technique[8] previously employed in studying these materials systems. The 3D method offers numerous advantages over the V_{OC} transient technique, including that it requires no fast electronics or optics, and it offers the full picture of transport and recombination as well as the consequent diffusion length. Additionally, meaningful quantitative comparisons can be made between relative parameter values measured for a variety of materials.

CONCLUSION

In summary, we have demonstrated two techniques that give direct insight into diffusion length in CQD solids. The two models agree in their quantitative determinations of diffusion length to within experimental error. Diffusion lengths as high as 80 nm were extracted; results that help explain recent progress in solar cells based on hybrid-passivated CQD solids. The diffusion-length-measuring methods described herein

offer a facile and rapid means of screening newly proposed chemistries and processes to advance the performance of CQD solids, without the need for full device architecture being developed.

METHODS

Materials Preparation. PbS CQDs of varying bandgaps and sizes (1.3 and 0.95 eV) are fabricated following published recipes.[8,32] Both PbS and $CdCl_2$ treated PbS CQDs are synthesized, purified with a 3× methanol precipitation, and redispersed on octane at a final concentration of 50 mg/mL.

Film Fabrication. Layer-by-layer spin-coating was applied to fabricate the CQD film on ITO substrates. Ligands were dissolved in methanol at 1% (by volume) for MPA and 10 mg/mL for tetrabutyl ammonium iodide (TBAI, iodine source). For p-type film fabrication,[1] the MPA ligand was used and fabrication proceeds in air with both standard and $CdCl_2$ treated PbS CQds (1) two drops of PbS CQDs in octane (50 mg mL^{-1}) were dropped onto substrates and were spin-cast at 2500 rpm for 10 s; (2) 0.75 mL of ligand solution was deposited, soaked for 3 s, followed by spin-coating 10 s at 2500 rpm; (3) 0.75 mL of methanol were dropped and spin-cast at 2500 rpm for 10 s, twice, to rinse the film. For n-type films,[38] the TBAI ligand was used in an oxygen-free nitrogen glovebox, following a similar procedure to the above but with a ligand soak time of 1 min per layer, and employing the PbS CQDs only. For the 1D scenario, donor layers of varying thicknesses were fabricated first, followed by a single capping layer of small bandgap CQDs. For the 3D scenario, CQD mixes were carefully prepared at different mass concentrations, and the masses of differently sized CQDs were taken into consideration in the analysis of the data.[45] Films were fabricated to be a total thickness of approximately 150 nm. Thickness measurements were carried out with a DekTak 3 profilometer averaging over several samples.

Optical Measurements. Samples were illuminated through the glass side using either a 428 nm diode laser with a 1 mm spot size for the 1D scenario at an intensity of approximately 0.1 W/cm^2 or a 632 nm diode laser for the 3D scenario to ensure more uniform generation. Measurements were performed in a controlled inert atmosphere by purging with N_2 gas. Collection was carried out using an Ocean Optics NIR512 spectrometer coupled to a focusing lens and 900 nm long pass filter through an optical fiber. α coefficients were measured on each type of film with ellipsometry used in fitting the data in the 1D model.

Conflict of Interest: The authors declare no competing financial interest.

Acknowledgment. This publication is based in part on work supported by Award KUS-11-009-21, made by King Abdullah University of Science and Technology (KAUST), by the Ontario Research Fund Research Excellence Program, and by the Natural Sciences and Engineering Research Council (NSERC) of Canada. David Zhitomirsky would like to acknowledge his NSERC CGS D scholarship. We thank Angstrom Engineering, Inc. and Innovative Technology, Inc. for useful discussions regarding material deposition methods and control of the glovebox environment, respectively. The authors would like to acknowledge P. Maraghechi for aid in ellipsometry measurements and technical assistance from E. Palmiano, R. Wolowiec, and D. Kopilovic.

Supporting Information Available: Additional 1D model details, 3D model analysis and parameters, and explanation of energy transfer *versus* charge diffusion. This material is available free of charge *via* the Internet at http://pubs.acs.org.

REFERENCES AND NOTES

1. Son, D. I.; Kwon, B. W.; Park, D. H.; Seo, W. S.; Yi, Y.; Angadi, B.; Lee, C. L.; Choi, W. K. Emissive ZnO-graphene Quantum Dots for White-Light-emitting Diodes. *Nat. Nanotechnol.* **2012**, *7*, 465–471.
2. Sun, L.; Choi, J. J.; Stachnik, D.; Bartnik, A. C.; Hyun, B.-R.; Malliaras, G. G.; Hanrath, T.; Wise, F. W. Bright Infrared Quantum-Dot Light-emitting Diodes Through Inter-Dot Spacing Control. *Nat. Nanotechnol.* **2012**, *7*, 369–373.
3. Shirasaki, Y.; Supran, G. J.; Bawendi, M. G.; Bulović, V. Emergence of Colloidal Quantum-Dot Light-emitting Technologies. *Nat. Photon.* **2012**, *7*, 13–23.
4. Konstantatos, G.; Howard, I.; Fischer, A.; Hoogland, S.; Clifford, J.; Klem, E.; Levina, L.; Sargent, E. H. Ultrasensitive Solution-Cast Quantum Dot Photodetectors. *Nature* **2006**, *442*, 180–183.
5. Konstantatos, G.; Badioli, M.; Gaudreau, L.; Osmond, J.; Bernechea, M.; de Arquer, F. P. G.; Gatti, F.; Koppens, F. H. L. Hybrid Graphene-Quantum Dot Phototransistors with Ultrahigh Gain. *Nat. Nanotechnol.* **2012**, *7*, 363–368.
6. Sargent, E. Photodetectors: A Sensitive Pair. *Nat. Nanotechnol.* **2012**, *7*, 349–350.
7. Tang, J.; Liu, H.; Zhitomirsky, D.; Hoogland, S.; Wang, X.; Furukawa, M.; Levina, L.; Sargent, E. H. Quantum Junction Solar Cells. *Nano Lett.* **2012**, *12*, 4889–4894.
8. Ip, A. H.; Thon, S. M.; Hoogland, S.; Voznyy, O.; Zhitomirsky, D.; Debnath, R.; Levina, L.; Rollny, L. R.; Carey, G. H.; Fischer, A.; *et al.* Hybrid Passivated Colloidal Quantum Dot Solids. *Nat. Nanotechnol.* **2012**, *7*, 577–582.
9. Semonin, O. E.; Luther, J. M.; Choi, S.; Chen, H.-Y.; Gao, J.; Nozik, A. J.; Beard, M. C. Peak External Photocurrent Quantum Efficiency Exceeding 100% via MEG in a Quantum Dot Solar Cell. *Science* **2011**, *334*, 1530–1533.
10. Tang, J.; Kemp, K. W.; Hoogland, S.; Jeong, K. S.; Liu, H.; Levina, L.; Furukawa, M.; Wang, X.; Debnath, R.; Cha, D.; *et al.* Colloidal-Quantum-Dot Photovoltaics Using Atomic-Ligand Passivation. *Nat. Mater.* **2011**, *10*, 765–771.
11. Talgorn, E.; Gao, Y.; Aerts, M.; Kunneman, L. T.; Schins, J. M.; Savenije, T.; van Huis, M. A.; van der Zant, H. S. J.; Siebbeles, L. D. A.; Houtepen, A. J. Unity Quantum Yield of Photogenerated Charges and Band-Like Transport in Quantum-Dot Solids. *Nat. Nanotechnol.* **2011**, *6*, 733–739.
12. Choi, J. J.; Luria, J.; Hyun, B. R.; Bartnik, A. C.; Sun, L.; Lim, Y. F.; Marohn, J. A.; Wise, F. W.; Hanrath, T. Photogenerated Exciton Dissociation in Highly Coupled Lead Salt Nanocrystal Assemblies. *Nano Lett.* **2010**, *10*, 1805–1811.
13. Bisquert, J. Interpretation of Electron Diffusion Coefficient in Organic and Inorganic Semiconductors with Broad Distributions of States. *Phys. Chem. Chem. Phys.* **2008**, *10*, 3175–3194.
14. Anta, J. A.; Mora-Seró, I.; Dittrich, T.; Bisquert, J. Interpretation of Diffusion Coefficients in Nanostructured Materials from Random Walk Numerical Simulation. *Phys. Chem. Chem. Phys.* **2008**, *10*, 4478–4485.
15. Guyot-Sionnest, P. Electrical Transport in Colloidal Quantum Dot Films. *J. Phys. Chem. Lett.* **2012**, *3*, 1169–1175.
16. Johnston, K. W.; Pattantyus-Abraham, A. G.; Clifford, J. P.; Myrskog, S. H.; Hoogland, S.; Shukla, H.; Klem, E. J. D.; Levina, L.; Sargent, E. H. Efficient Schottky-Quantum-Dot Photovoltaics: The Roles of Depletion, Drift, and Diffusion. *Appl. Phys. Lett.* **2008**, *92*, 122111.
17. Nag, A.; Chung, D. S.; Dolzhnikov, D. S.; Dimitrijevic, N. M.; Chattopadhyay, S.; Shibata, T.; Talapin, D. V. The Effect of Metal Ions on Photoluminescence, Charge Transport, Magnetic and Catalytic Properties of All-Inorganic Colloidal Nanocrystals and Nanocrystal Solids. *J. Am. Chem. Soc.* **2012**, *134*, 13604–13615.
18. Talapin, D. V.; Murray, C. B. PbSe Nanocrystal Solids for n- and p-Channel Thin Film Field-Effect Transistors. *Science* **2005**, *310*, 86–89.
19. Choi, J.-H.; Fafarman, A. T.; Oh, S. J.; Ko, D.-K.; Kim, D. K.; Diroll, B. T.; Muramoto, S.; Gillen, J. G.; Murray, C. B.; Kagan, C. R. Bandlike Transport in Strongly Coupled and Doped Quantum Dot Solids: A Route to High-Performance Thin-Film Electronics. *Nano Lett.* **2012**, *12*, 2631–2638.

20. Jeong, K. S.; Tang, J.; Liu, H.; Kim, J.; Schaefer, A. W.; Kemp, K.; Levina, L.; Wang, X.; Hoogland, S.; Debnath, R.; *et al.* Enhanced Mobility-Lifetime Products in PbS Colloidal Quantum Dot Photovoltaics. *ACS Nano* **2011**, *6*, 89–99.
21. Moreels, I.; Lambert, K.; Smeets, D.; Muynck, D. De; Nollet, T.; Martins, J. C.; Vanhaecke, F.; Vantomme, A.; Delerue, C.; Allan, G.; *et al.* Size-Dependent Optical Properties of Colloidal PbS Quantum Dots. *ACS Nano* **2009**, *3*, 3023–3030.
22. Gao, Y.; Aerts, M.; Sandeep, C. S. S.; Talgorn, E.; Savenije, T. J.; Kinge, S.; Siebbeles, L. D. A.; Houtepen, A. J. Photoconductivity of PbSe Quantum-Dot Solids: Dependence on Ligand Anchor Group and Length. *ACS Nano* **2012**, *6*, 9606–9614.
23. Ota, T.; Oe, K.; Yamaguchi, M. Determination of Electron Diffusion Length from Photoluminescence Measurements in $In_xGa_{1-x}As$ Junctions. *J. Appl. Phys.* **1975**, *46*, 3674–3675.
24. Ettenberg, M.; Kressel, H.; Gilbert, S. L. Minority Carrier Diffusion Length and Recombination Lifetime in GaAs:Ge Prepared by Liquid-Phase Epitaxy. *J. Appl. Phys.* **1973**, *44*, 827–831.
25. Gourley, P. L.; Biefeld, R. M.; Zipperian, T. E.; Wiczer, J. J. Minority-carrier Diffusion Lengths in $GaP/GaAs_xP_{1-x}$ Strained-layer Superlattices. *Appl. Phys. Lett.* **1984**, *44*, 983–985.
26. Luke, K. L.; von Roos, O.; Cheng, L. Quantification of the Effects of Generation Volume, Surface Recombination Velocity, and Diffusion Length on the Electron-Beam-Induced Current and Its Derivative: Determination of Diffusion Lengths in the Low Micron and Submicron Ranges. *J. Appl. Phys.* **1985**, *57*, 1978–1984.
27. Jin, M.-J.; Chen, X.-Y.; Gao, Z.-M.; Ling, T.; Du, X.-W. Improved Photo-Electron Conversion Efficiency of ZnO/CdS Coaxial Nanorods by p-Type CdTe Coating. *Nanotechnology* **2012**, *23*, 485401.
28. Kroeze, J. E.; Savenije, T. J.; Vermeulen, M. J. W.; Warman, J. M. Contactless Determination of the Photoconductivity Action Spectrum, Exciton Diffusion Length, and Charge Separation Efficiency in Polythiophene-Sensitized TiO_2 Bilayers. *J. Phys. Chem. B* **2003**, *107*, 7696–7705.
29. Quist, P. A. C.; Savenije, T. J.; Schins, J. M.; Kroeze, J. E.; Rijkers, P. A.; Siebbeles, L. D. A. Electron Diffusion in Polymer:Fullerene Bulk Heterojunctions. *Phys. Rev. B* **2007**, *75*, 195317.
30. Pattantyus-Abraham, A. G.; Kramer, I. J.; Barkhouse, A. R.; Wang, X.; Konstantatos, G.; Debnath, R.; Levina, L.; Raabe, I.; Nazeeruddin, M. K.; Gratzel, M.; *et al.* Depleted-Heterojunction Colloidal Quantum Dot Solar Cells. *ACS Nano* **2010**, *4*, 3374–3380.
31. McKelvey, J. *Solid State and Semiconductor Physics*; Krieger Pub Co.: Malabar, FL, 1982; pp 320−335.
32. Hines, M. A.; Scholes, G. D. Colloidal PbS Nanocrystals with Size-Tunable Near-Infrared Emission: Observation of Post-Synthesis Self-Narrowing of the Particle Size Distribution. *Adv. Mater.* **2003**, *15*, 1844–1849.
33. Kramer, I. J.; Levina, L.; Debnath, R.; Zhitomirsky, D.; Sargent, E. H. Solar Cells Using Quantum Funnels. *Nano Lett.* **2011**, *11*, 3701–3706.
34. Xu, F.; Ma, X.; Haughn, C. R.; Benavides, J.; Doty, M. F.; Cloutier, S. G. Efficient Exciton Funneling in Cascaded PbS Quantum Dot Superstructures. *ACS Nano* **2011**, *5*, 9950–9957.
35. Menke, S. M.; Luhman, W. A.; Holmes, R. J. Tailored Exciton Diffusion in Organic Photovoltaic Cells for Enhanced Power Conversion Efficiency. *Nat. Mater.* **2012**, *12*, 152–157.
36. Lunt, R. R.; Benziger, J. B.; Forrest, S. R. Relationship Between Crystalline Order and Exciton Diffusion Length in Molecular Organic Semiconductors. *Adv. Mater.* **2010**, *22*, 1233–1236.
37. Nordin, M.; Li, J.; Clowes, S.; Curry, R. Temperature Dependent Optical Properties of PbS Nanocrystals. *Nanotechnology* **2012**, *23*, 275701.
38. Zhitomirsky, D.; Furukawa, M.; Tang, J.; Stadler, P.; Hoogland, S.; Voznyy, O.; Liu, H.; Sargent, E. H. N-Type Colloidal-Quantum-Dot Solids for Photovoltaics. *Adv. Mater.* **2012**, *24*, 6181–6185.
39. Zhitomirsky, D.; Kramer, I. J.; Labelle, A. J.; Fischer, A.; Debnath, R.; Pan, J.; Bakr, O. M.; Sargent, E. H. Colloidal Quantum Dot Photovoltaics: The Effect of Polydispersity. *Nano Lett.* **2012**, *12*, 1007–1012.
40. Kagan, C. R.; Murray, C. B.; Nirmal, M.; Bawendi, M. G. Electronic Energy Transfer in CdSe Quantum Dot Solids. *Phys. Rev. Lett.* **1996**, *76*, 1517–1520.
41. Luhman, W. A.; Holmes, R. J. Enhanced Exciton Diffusion in an Organic Photovoltaic Cell by Energy Transfer Using a Phosphorescent Sensitizer. *Appl. Phys. Lett.* **2009**, *94*, 153304.
42. Kramer, I. J.; Sargent, E. H. Colloidal Quantum Dot Photovoltaics: A Path Forward. *ACS Nano* **2011**, *5*, 8506–8514.
43. Gao, J.; Johnson, J. C. Charge Trapping in Bright and Dark States of Coupled PbS Quantum Dot Films. *ACS Nano* **2012**, *6*, 3292–3303.
44. Liu, Y.; Gibbs, M.; Puthussery, J.; Gaik, S.; Ihly, R.; Hillhouse, H. W.; Law, M. Dependence of Carrier Mobility on Nanocrystal Size and Ligand Length in PbSe Nanocrystal Solids. *Nano Lett.* **2010**, *10*, 1960–1969.
45. Moreels, I.; Lambert, K.; Muynck, D. De; Vanhaecke, F.; Poelman, D.; Martins, J. C.; Allan, G.; Hens, Z. Composition and Size-Dependent Extinction Coefficient of Colloidal PbSe Quantum Dots. *Chem. Mater.* **2007**, *19*, 6101–6106.
46. O'Regan, B. C.; Scully, S.; Mayer, A. C.; Palomares, E.; Durrant, J. The Effect of Al_2O_3 Barrier Layers in TiO_2/Dye/CuSCN Photovoltaic Cells Explored by Recombination and DOS Characterization Using Transient Photovoltage Measurements. *J. Phys. Chem. B* **2005**, *109*, 4616–4623.
47. Shuttle, C. G.; O'Regan, B.; Ballantyne, A. M.; Nelson, J.; Bradley, D. D. C.; de Mello, J.; Durrant, J. R. Experimental Determination of the Rate Law for Charge Carrier Decay in a Polythiophene: Fullerene Solar Cell. *Appl. Phys. Lett.* **2008**, *92*, 093311.